# Large-eddy simulations of turbulent thermal convection using renormalized viscosity and thermal diffusivity

Sumit Vashishtha* and Mahendra K. Verma†
*Department of Physics, Indian Institute of Technology, Kanpur 208016, India*

Roshan Samuel‡
*Department of Mechanical Engineering, Indian Institute of Technology, Kanpur 208016, India*

(Received 7 May 2018; revised manuscript received 31 July 2018; published 24 October 2018)

In this paper we employ renormalized viscosity and thermal diffusivity to construct a subgrid-scale model for large eddy simulation (LES) of turbulent thermal convection. For LES, we add $\nu_{\rm ren} \propto \Pi_u^{1/3}(\pi/\Delta)^{-4/3}$ to the kinematic viscosity; here $\Pi_u$ is the turbulent kinetic energy flux, and $\Delta$ is the grid spacing. We take subgrid thermal diffusivity to be same as the subgrid kinematic viscosity. We performed LES of turbulent thermal convection on a $128^3$ grid and compare the results with those obtained from direct numerical simulation (DNS) on a $512^3$ grid. We started the DNS with random initial condition and forked a LES simulation using the large wave number modes of DNS initial condition. Though the Nusselt number is overestimated in LES as compared to that in DNS, there is a good agreement between the LES and DNS results on the evolution of kinetic energy and entropy, spectra and fluxes of velocity and temperature fields, and the isosurfaces of temperature.

DOI: 10.1103/PhysRevE.98.043109

## I. INTRODUCTION

Turbulence is one of the most difficult phenomena to simulate on a computer due to the vast range of length scales involved. In a direct numerical simulation (DNS), all the length scales of the flow need to be resolved, which is very challenging for large Reynolds numbers. This problem is circumvented in large eddy simulations (LES) where the small-scale fluctuations are modeled. Thus, only the large and intermediate scales need to be resolved in LES, which makes it computationally less expensive and practical compared to DNS.

In hydrodynamic turbulence, the velocity fields at different scales interact with each other and create a cascade of energy, called energy flux $\Pi_u$. The energy flux in the inertial regime equals the energy dissipation. Scaling analysis reveals that the effective viscosity at length scale $l$ is proportional to $\Pi_u^{1/3} l^{4/3}$; this viscosity enhances the diffusion of linear momentum. This feature is exploited in eddy-viscosity based subgrid-scale (SGS) models of LES.

The earliest SGS model was proposed by Smagorinsky [1], who modeled the effective viscosity as

$$\nu_{\rm Smag} = (C_s\Delta)^2\sqrt{2\bar{S}_{ij}\bar{S}_{ij}}, \tag{1}$$

where $\bar{S}_{ij}$ is the stress tensor at the resolved scales, $\Delta$ is the smallest grid scale, and $C_s$ is a constant that is taken between 0.1 and 0.2. A less popular but theoretically rigorous LES model is based on the renormalized viscosity. Using renormalization group (RG) analysis, Yakhot and Orszag [2], McComb and Watt [3], McComb [4,5], Zhou *et al.* [6], Zhou [7] estimated the effective viscosity. In one of the computations, McComb and colleagues [3–5] showed that the renormalized viscosity is

$$\nu_{\rm ren}(k) = K_{\rm Ko}^{1/2}\Pi^{1/3}k^{-4/3}\nu_*, \tag{2}$$

where $K_{\rm Ko}$ is Kolmogorov's constant, and $\nu_*$ is a constant. Using a RG computation, McComb and Watt [3] found that $\nu_* \approx 0.50$ and $K_{\rm Ko} \approx 1.62$, while Verma [8] computed the above quantities using a refined technique and found $\nu_* \approx 0.38$ and $K_{\rm Ko} \approx 1.6$. In LES it is assumed that the length scale corresponding to the grid spacing, $\Delta$, lies in the inertial range where the energy spectrum $E_u(k) \sim k^{-5/3}$, and the effective viscosity follows Eq. (2) with $k = k_c = \pi/\Delta$. Refer to Verma and Kumar [9] and Vashishtha *et al.* [10] for LES of hydrodynamic turbulence using renormalized viscosity.

Turbulent thermal convection is more complex [11–13] than hydrodynamic turbulence due to the presence of another field (temperature) and thermal plates. In this paper, we limit our attention to an idealised version of thermal convection called *Rayleigh-Bénard convection* (RBC) in which a Boussinesq fluid is confined between two perfectly conducting thermal plates. Two important parameters for RBC are the Rayleigh number, Ra, that quantifies the strength of buoyancy compared to the viscous effects, and the Prandtl number, Pr, which is a ratio of kinematic viscosity and thermal diffusivity. RBC has been studied widely using experiments, numerical simulations, and modeling. Here we describe some of the leading numerical results.

First, we review DNS of turbulent thermal convection. Using finite difference scheme, Stevens *et al.* [14] performed

*vash.sumit@gmail.com
†mkv@iitk.ac.in
‡roshanj@iitk.ac.in

 

a three-dimensional RBC simulation in a cylinder at extreme parameters: Ra $= 2 \times 10^{12}$ and Pr $= 0.7$. Shishkina *et al.* [15] and Shishkina and Thess [16] simulated turbulent thermal convection with Ra up to $10^{10}$ and studied the temperature profiles in the bulk and in the boundary layers. Shishkina *et al.* [17] quantified the viscous and thermal boundary layer thickness that are useful for modeling turbulent convection. Verma *et al.* [18] performed a very high-resolution spectral simulation for Ra $= 1.1 \times 10^{11}$ and Pr $= 1$ using free-slip boundary conditions. Kooij *et al.* [19] performed convergence tests on several codes for various grid refinements; they took Ra $= 10^8$ and Pr $= 1$ as test parameters. Zhu *et al.* [20], and Vincent and Yuen [21] performed two-dimensional RBC simulations for Ra up to $10^{14}$. Schumacher *et al.* [22] simulated turbulent RBC in a cylindrical geometry at low Prandtl numbers and studied the structures of temperature and velocity boundary layers. Chong *et al.* [23] investigated the effect of geometrical confinement on RBC for a wide range of Pr at a fixed Ra of $10^8$. They also deduced scaling relations for the optimal aspect ratio at which the heat transport (characterized by Nu) is significantly enhanced. We remark that in RBC, the boundary layers and flow structures become very thin at very large Ra, which require extreme spatial and temporal resolutions [24,25] in simulations. Therefore, DNS of RBC at extreme parameters is very difficult.

Another numerical approach is Reynolds-averaged Navier Stokes (RANS) [26]. Kenjereš and Hanjalic [27] used transient RANS (TRANS) wherein only the large and deterministic eddy structures are resolved in space and time. Using this approach, they simulated turbulent thermal convection up to Ra $= 10^{15}$. They obtained Nu $\sim$ Ra$^{0.31}$ till Ra $= 10^{13}$, beyond which the Nu-Ra scaling exponent tends to increase as observed in RBC experiments of Chavanne *et al.* [28] and He *et al.* [29]. These implications, however, remain unclear due to low spatial resolution of numerical schemes at such high Ra [11].

Excessive resource requirements make DNS of RBC at extreme Ra very impractical. For such problems, LES offers an interesting alternative. However, there is no consensus on SGS models of RBC. For LES of RBC, we need to model the effective viscosity and thermal diffusivity at subgrid scales [see Eq. (1)]. The ratio of effective viscosity and effective thermal diffusivity is called the turbulent Prandtl number (Pr$_{\rm turb}$). In the following we list some of the LES models of turbulent thermal convection.

Eidson [30] and Huang *et al.* [31] constructed LES models for turbulent thermal convection along similar lines as in Smagorinsky's eddy-viscosity model for hydrodynamic turbulence. They proposed that Pr$_{\rm turb} \approx 0.4$. The turbulent Prandtl number, however, varies at different regions of the flow, e.g., in boundary layer and bulk. Considering these factors, Dabbagh *et al.* [32] argued that Pr$_{\rm turb}$ could lie between 0.1 and 1. Sergent *et al.* [33] employed a mixed-scale diffusive model for their LES model. Wong and Lilly [34] used dynamic LES that suppresses excessive dissipation occurring in Smagorinsky's model. However, dynamic LES itself induces numerical instabilities due to spatial averaging during the evaluation of model parameters. Foroozani *et al.* [35] overcame these issues by employing a Lagrangian dynamic SGS model [36] and studied reorientations of the large scale structures in turbulent thermal convection.

Kimmel and Domaradzki [37] constructed an LES model wherein the SGS quantities are estimated by expanding the temperature and velocity fields to scales smaller than the grid size. Shishkina and Wagner [38,39] performed LES using a tensor-diffusivity SGS model [40] wherein SGS stress tensors are approximated using series expansions for the filtered products. We remark that in most of these models, the Nusselt number is overpredicted compared to their DNS counterpart [30,32,34,37]; this increase can be attributed to the lack of backscatter modeling in such models. Backscatter is the energy transfer to large scales from subgrid scales [41].

In the LES models described above, the effective viscosity and thermal diffusivity are chosen either by trial and error or by phenomenological arguments. In the present paper, we attempt to derive these quantities using field theory, and we construct an SGS model for turbulent thermal convection using renormalized parameters. Researchers [2] have performed RG computation of passive scalar turbulence, but its applicability to turbulent thermal convection is highly debatable due to the additional complexities arising due to walls and buoyancy [12,13,18]. In thermal convection, buoyancy drives the flow, and the mean temperature gradient affects the thermal fluctuations in a nontrivial manner. It was generally believed that RBC is anisotropic due to the directional dependence arising from gravity. Recent works [18,42], however, show that in RBC, the degree of anisotropy is quite limited. We provide further details next.

L'vov [43], L'vov and Falkovich [44], and Rubinstein [45] employed field-theoretic tools to model turbulent thermal convection and argued that its kinetic energy spectrum follows Bolgiano-Obukhov scaling: $E_u(k) \sim k^{-11/5}$ and $\nu(k) \sim k^{-8/5}$. Recent theoretical arguments and numerical simulations [18,46], however, show that turbulent thermal convection has properties similar to hydrodynamic turbulence: $E_u(k) \sim k^{-5/3}$ and $\nu(k) \sim k^{-4/3}$. Nath *et al.* [42] and Verma *et al.* [18] also show that turbulent thermal convection is nearly isotropic, and the energy transfers in such flows are local and forward. We construct an LES of turbulent thermal convection based on these observations.

Due to the aforementioned similarities between the hydrodynamic turbulence and turbulent thermal convection, we employ renormalized viscosity of the form of Eq. (2) for turbulent convection. Though temperature field in thermal convection has relatively complex behavior, for simplicity, we take $\kappa(k) = \nu(k)$ or turbulent Prandtl number Pr$_{\rm turb} = 1$.

We perform LES on a $128^3$ grid with the aforementioned renormalized parameters and compare its results with that of DNS on a $512^3$ grid. We show that the evolution of the total kinetic energy and entropy, as well as the spectra and fluxes of the temperature and velocity fields of DNS and LES, are approximately the same. The large-scale features of thermal plumes too are captured very well by our LES.

The outline of the paper is as follows: In Sec. II we detail our SGS model for the LES of turbulent thermal convection. Simulation details are discussed in Sec. III. Results obtained from the LES and DNS are compared in Sec. IV. We summarize our results in Sec. V.

## II. LES FORMULATIONS USING RENORMALIZED PARAMETERS

We consider a Boussinesq fluid confined between two horizontal plates that are separated by a distance $d$. The temperature difference between the two plates is $\Delta T$. This system, called Rayleigh-Bénard convection (RBC), is described by the following equations [47]:

$$\frac{\partial \mathbf{u}}{\partial t} + (\mathbf{u}\cdot\nabla)\mathbf{u} = -\frac{1}{\rho_0}\nabla\sigma + \alpha g\theta\hat{z} + \nu\nabla^2\mathbf{u}, \tag{3}$$

$$\frac{\partial \theta}{\partial t} + (\mathbf{u}\cdot\nabla)\theta = \frac{(\Delta T)}{d}u_z + \kappa\nabla^2\theta, \tag{4}$$

$$\nabla\cdot\mathbf{u} = 0, \tag{5}$$

where $\mathbf{u}$ is the velocity field, $\theta$ and $\sigma$ are, respectively, the temperature and pressure fluctuations from the conduction state, and $\hat{z}$ is the buoyancy direction. Here $\alpha$ is the thermal expansion coefficient, $g$ is the acceleration due to gravity, and $\rho_0$, $\nu$, $\kappa$ are the mean density, kinematic viscosity, and thermal diffusivity of the fluid, respectively. We nondimensionalize Eqs. (3), (4), and (5) using the temperature difference between the two plates ($\Delta T$) as the temperature scale, the plates separation $d$ as the length scale, and the free-fall velocity, $\sqrt{\alpha g(\Delta T)d}$, as the velocity scale. This yields the following system of equations:

$$\frac{\partial \mathbf{u}}{\partial t} + (\mathbf{u}\cdot\nabla)\mathbf{u} = -\nabla\sigma + \theta\hat{z} + \sqrt{\frac{\mathrm{Pr}}{\mathrm{Ra}}}\nabla^2\mathbf{u}, \tag{6}$$

$$\frac{\partial \theta}{\partial t} + (\mathbf{u}\cdot\nabla)\theta = u_z + \frac{1}{\sqrt{\mathrm{RaPr}}}\nabla^2\theta, \tag{7}$$

$$\nabla\cdot\mathbf{u} = 0, \tag{8}$$

where the Prandtl number

$$\mathrm{Pr} = \frac{\nu}{\kappa} \tag{9}$$

and the Rayleigh number

$$\mathrm{Ra} = \frac{\alpha g(\Delta T)d^3}{\nu\kappa} \tag{10}$$

are two nondimensional parameters.

Representation of flow properties at various scales is more convenient in Fourier space. Using the definition of the Fourier transform,

$$\mathbf{u}(\mathbf{x}) = \sum_{\mathbf{k}} \hat{\mathbf{u}}(\mathbf{k})e^{i\mathbf{k}\cdot\mathbf{x}}, \tag{11}$$

$$\theta(\mathbf{x}) = \sum_{\mathbf{k}} \hat{\theta}(\mathbf{k})e^{i\mathbf{k}\cdot\mathbf{x}}, \tag{12}$$

we derive the RBC equations in Fourier space as

$$\frac{d}{dt}\hat{\mathbf{u}}(\mathbf{k}) + \hat{\mathbf{N}}_{\mathbf{u}}(\mathbf{k}) = -i\frac{1}{\rho_0}\mathbf{k}\hat{\sigma}(\mathbf{k}) + \alpha g\hat{\theta}(\mathbf{k})\hat{z} - k^2\nu\hat{\mathbf{u}}(\mathbf{k}), \tag{13}$$

$$\frac{d}{dt}\hat{\theta}(\mathbf{k}) + \hat{N}_\theta(\mathbf{k}) = \frac{(\Delta T)}{d}\hat{u}_z(\mathbf{k}) - k^2\kappa\hat{\theta}(\mathbf{k}), \tag{14}$$

$$\mathbf{k}\cdot\hat{\mathbf{u}}(\mathbf{k}) = 0, \tag{15}$$

where the nonlinear terms are

$$\hat{\mathbf{N}}_{\mathbf{u}}(\mathbf{k}) = \sum_{\mathbf{p}}[\mathbf{k}\cdot\hat{\mathbf{u}}(\mathbf{q})]\hat{\mathbf{u}}(\mathbf{p}), \tag{16}$$

$$\hat{N}_\theta(\mathbf{k}) = \sum_{\mathbf{p}}[\mathbf{k}\cdot\hat{\mathbf{u}}(\mathbf{q})]\hat{\theta}(\mathbf{p}), \tag{17}$$

with $\mathbf{p}+\mathbf{q}=\mathbf{k}$. The nonlinear terms of Eqs. (16, 17) represent the triadic interactions among the wave numbers $(\mathbf{k},\mathbf{p},\mathbf{q})$ that satisfy $\mathbf{p}+\mathbf{q}=\mathbf{k}$ and are numerically computed using fast Fourier transforms. In Fourier space, the pressure is computed using

$$\hat{\sigma}(\mathbf{k}) = \frac{i}{k^2}[\mathbf{k}\cdot\hat{\mathbf{N}}_u(\mathbf{k}) - \alpha g k_z\hat{\theta}(\mathbf{k})]. \tag{18}$$

In RG analysis of fluid turbulence, the Fourier modes of wave number shells are truncated iteratively [2–7], which leads to an elimination of some of the triadic interactions. In RG procedure, these eliminated interactions are taken into account by an enhanced viscosity. For hydrodynamic turbulence, it has been shown that the total effective viscosity at wave number $k_c$ is

$$\nu_{\mathrm{tot}} = \nu + \nu_{\mathrm{ren}}(k_c) = \nu + K_{\mathrm{Ko}}^{1/2}\Pi_u^{1/3}k_c^{-4/3}\nu_*, \tag{19}$$

with $\nu_* = 0.38$. Here $\nu_{\mathrm{ren}}(k_c)$ is the renormalized viscosity that is added to the original kinematic viscosity. The above derivation assumes Kolmogorov's spectrum for the kinetic energy:

$$E_u(k) = K_{\mathrm{Ko}}\Pi_u^{2/3}k^{5/3}. \tag{20}$$

The equation for the energy flux yields Kolmogorov's constant as approximately 1.6.

For passive scalar turbulence, Yakhot and Orszag [2], and Verma [48] performed RG analysis and deduced that

$$\kappa_{\mathrm{tot}} = \kappa + \kappa_{\mathrm{ren}}(k) = \kappa + K_{\mathrm{Ko}}^{1/2}\Pi_u^{1/3}k_c^{-4/3}\kappa_*, \tag{21}$$

$$E_\theta(k) = \mathrm{Ba}\Pi_\theta\Pi_u^{-1/3}k^{-5/3}. \tag{22}$$

Verma [48] reported that $\kappa_* = 0.85$, and the Batchelor's constant $\mathrm{Ba} = 1.25$, while Yakhot and Orszag [2] obtained $\kappa_*/\nu_* = 0.85$ and $\mathrm{Ba} = 1.16$. We define *turbulent Prandtl number* as the ratio of the turbulent viscosity and turbulent diffusivity, and *total Prandtl number* as the ratio of the total viscosity and total diffusivity:

$$\mathrm{Pr}_{\mathrm{turb}} = \frac{\nu_{\mathrm{ren}}(k)}{\kappa_{\mathrm{ren}}(k)}, \tag{23}$$

$$\mathrm{Pr}_{\mathrm{tot}} = \frac{\nu_{\mathrm{tot}}}{\kappa_{\mathrm{tot}}} = \frac{\nu+\nu_{\mathrm{ren}}(k)}{\kappa+\kappa_{\mathrm{ren}}(k)}. \tag{24}$$

In the inertial range of the turbulent convection, $\nu \ll \nu_{\mathrm{ren}}(k)$ and $\kappa \ll \kappa_{\mathrm{ren}}(k)$. Hence,

$$\mathrm{Pr}_{\mathrm{tot}} = \frac{\nu_{\mathrm{tot}}}{\kappa_{\mathrm{tot}}} \approx \frac{\nu_{\mathrm{ren}}(k)}{\kappa_{\mathrm{ren}}(k)} = \frac{\nu_*}{\kappa_*} = \mathrm{Pr}_{\mathrm{turb}}. \tag{25}$$

Note that $\nu/\kappa$ is the *molecular Prandtl number*, and we denote it by Pr. Clearly, $\mathrm{Pr}_{\mathrm{turb}} \approx 0.7179$ and 0.45, respectively, for Yakhot and Orszag [2]'s and Verma [48]'s parameters.

Turbulent thermal convection, however, is more complex than passive scalar turbulence. Kumar *et al.* [46] and Verma *et al.* [18] showed that the kinetic energy spectrum of turbulent thermal convection is very similar to that of hydrodynamic turbulence ($\sim k^{-5/3}$), but the temperature field exhibits a bispectrum with one branch as $k^{-2}$ [18,49]. Verma *et al.* [18] and Nath *et al.* [42] showed that turbulent thermal convection is nearly isotropic in Fourier space, and that the energy transfers in Fourier space is local and forward, similar to that in hydrodynamic turbulence. Borue and Orszag [50] arrived at similar conclusions in their analysis. Though there have been several attempts at field-theoretic treatment of thermal convection [43–45], there is no rigorous RG analysis of turbulent thermal convection that is consistent with the observations of Kumar *et al.* [46] and Verma *et al.* [18].

In absence of any analytical input on the renormalized viscosity and thermal diffusivity of turbulent thermal convection, we use the models proposed by earlier researchers. Motivated by the numerical observations of Kumar *et al.* [46], Verma *et al.* [18], and Verma [13] that the properties of turbulent thermal convection are similar to hydrodynamic turbulence, we model the viscosity in turbulent thermal convection as in Eq. (19). Eidson [30] proposed that $\mathrm{Pr_{turb}} \approx 0.4$, while Dabbagh *et al.* [32] stated that $\mathrm{Pr_{turb}}$ could lie between 0.1 and 1 depending on the scenario. For example, $\mathrm{Pr_{turb}}$ in the boundary layer and in the bulk is likely to be different. For our LES simulation, for simplicity, we assume that

$$\kappa_{\rm ren}(k) = \nu_{\rm ren}(k) \tag{26}$$

or that the turbulent Prandtl number is unity. In the forthcoming sections, we employ the above model for the LES of turbulent thermal convection problem and compare its performance with DNS.

The above scheme is expected to work well for moderate molecular Prandtl numbers $\nu/\kappa$, that is, for $0.1 < \nu/\kappa < 10$. For very small molecular Prandtl numbers, the temperature equation becomes linear, while the equation for the velocity field becomes linear for large molecular Prandtl numbers. Hence, we need to make appropriate corrections to the above LES schemes. These simulations will be taken up in the future.

For our LES scheme, we employ sharp spectral filter at cutoff wave number $k_c$:

$$\hat{\bar{\mathbf{u}}}(\mathbf{k}) = H(k_c - k)\hat{\mathbf{u}}(\mathbf{k}), \tag{27}$$

$$\hat{\bar{\theta}}(\mathbf{k}) = H(k_c - k)\hat{\theta}(\mathbf{k}), \tag{28}$$

where $H$ represents the Heaviside function, and $k_c = \pi/\Delta$, where $\Delta$ is the subgrid cutoff in real space. Under this scheme, the real space velocity and temperature fluctuations are

$$\bar{\mathbf{u}}(\mathbf{x}) = \sum_{\mathbf{k}} e^{i\mathbf{k}\cdot\mathbf{x}}\hat{\bar{\mathbf{u}}}(\mathbf{k}) = \sum_{|\mathbf{k}|<|\mathbf{k_c}|} e^{i\mathbf{k}\cdot\mathbf{x}}\hat{\mathbf{u}}(\mathbf{k}), \tag{29}$$

$$\bar{\theta}(\mathbf{x},t) = \sum_{\mathbf{k}} e^{i\mathbf{k}\cdot\mathbf{x}}\hat{\bar{\theta}}(\mathbf{k}) = \sum_{|\mathbf{k}|<|\mathbf{k_c}|} e^{i\mathbf{k}\cdot\mathbf{x}}\hat{\theta}(\mathbf{k}). \tag{30}$$

Under these assumptions, the equations for the resolved Fourier modes are

$$\frac{d}{dt}\hat{\bar{\mathbf{u}}}(\mathbf{k}) + \hat{\bar{\mathbf{N}}}'_{\mathbf{u}}(\mathbf{k}) = -i\mathbf{k}\frac{1}{\rho_0}\hat{\bar{\sigma}}(\mathbf{k}) + \hat{\bar{\theta}}(\mathbf{k})\hat{z} - k^2\nu_{\rm tot}\hat{\bar{\mathbf{u}}}(\mathbf{k}), \tag{31}$$

$$\frac{d}{dt}\hat{\bar{\theta}}(\mathbf{k}) + \hat{\bar{N}}'_{\theta}(\mathbf{k}) = \frac{(\Delta T)}{d}\hat{\bar{u}}_z(\mathbf{k}) - k^2\kappa_{\rm tot}\hat{\bar{\theta}}(\mathbf{k}), \tag{32}$$

$$\mathbf{k}\cdot\hat{\bar{\mathbf{u}}}(\mathbf{k}) = 0, \tag{33}$$

where

$$\hat{\bar{\mathbf{N}}}'_{\mathbf{u}}(\mathbf{k}) = \sum_{|\mathbf{k}|,|\mathbf{p}|,|\mathbf{q}|<k_c} [\mathbf{k}\cdot\hat{\bar{\mathbf{u}}}(\mathbf{q})]\hat{\bar{\mathbf{u}}}(\mathbf{p}), \tag{34}$$

$$\hat{\bar{N}}'_{\theta}(\mathbf{k}) = \sum_{|\mathbf{k}|,|\mathbf{p}|,|\mathbf{q}|<k_c} [\mathbf{k}'\cdot\hat{\bar{\mathbf{u}}}(\mathbf{q})]\hat{\bar{\theta}}(\mathbf{k}'') \tag{35}$$

with $\mathbf{k} = \mathbf{p} + \mathbf{q}$. As discussed above, for LES, we employ Eqs. (19) and (26) for the effective viscosity and thermal diffusivity. In addition, we take $k_c = (2/3)(\pi/\Delta)$ with $\Delta$ as the grid spacing, which is uniform in our simulations. The factor 2/3 is discussed below.

Several important issues regarding LES implementation are in order. The computation of $\nu_{\rm tot}$ for LES requires the kinetic energy flux $\Pi_u(k_0)$, where $k_0$ is in the inertial range. In our simulations, we compute $\Pi_u(k_0)$ using the formula proposed by Verma [8] and Dar *et al.* [51]:

$$\Pi_u(k_0) = \sum_{k\geqslant k_0}\sum_{p<k_0} \mathrm{Im}[\mathbf{k}\cdot\mathbf{u}(\mathbf{q})][\mathbf{u}^*(\mathbf{k})\cdot\mathbf{u}(\mathbf{p})], \tag{36}$$

where $\mathbf{k} = \mathbf{p} + \mathbf{q}$,

We use a box of unit dimension and set the Fourier modes $|\mathbf{k}| > 2\pi N/3$ to zero. Hence, the nonzero Fourier modes are $k_i = [-2\pi N/3 : 2\pi N/3]$, where $i = x, y, z$. Therefore, the effective $k_{\rm max} = 2\pi N/3$. Note that $\Delta = 1/N$, hence

$$k_c = \frac{2}{3}\frac{\pi}{\Delta} = \frac{2}{3}N\pi. \tag{37}$$

Thus $k_c = k_{\rm max}$.

In Sec III we discuss the details of our numerical simulations.

## III. SIMULATION DETAILS

We employ a pseudospectral method for our numerical simulations and solve Eqs. (13)–(15) for DNS and Eqs. (31)–(33) for LES. The convection module of the code Tarang [52,53] is used to perform a DNS on $512^3$ grid and an LES on $128^3$ grid. As mentioned earlier, we take a box of unit size on which we employ 2/3 rule for dealiasing [54]. We apply free-slip and conducting boundary conditions at the top and bottom walls, along with periodic boundary conditions at the side walls.

For DNS with $\mathrm{Ra} = 10^8$ and molecular Prandtl number, $\mathrm{Pr} = 1$, we have

$$\nu_{\rm tot} = \kappa_{\rm tot} = \nu = \kappa = \sqrt{\mathrm{Pr/Ra}} = 10^{-4}, \tag{38}$$

and for LES, we take $k_c = 2\pi N/3$ with $N = 128$, and compute the viscosity and thermal diffusivity using Eqs. (19)

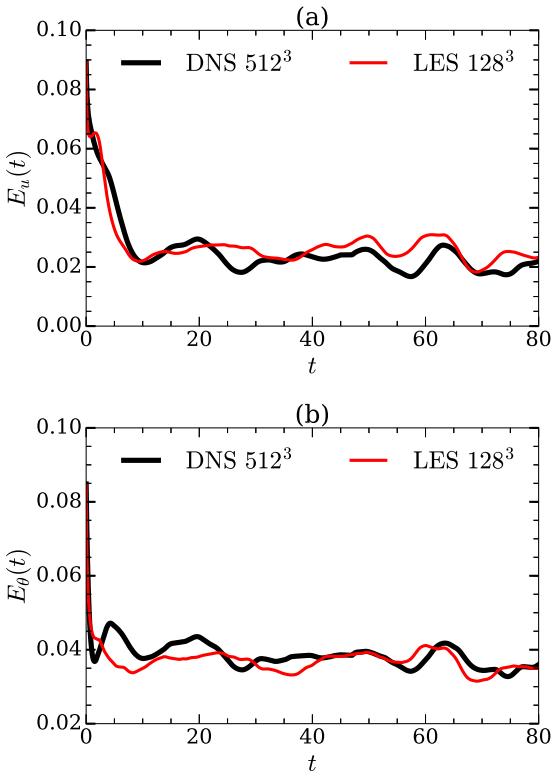


FIG. 1. Plots for LES on a $128^3$ grid (thin red lines) and DNS on a $512^3$ grid (thick black lines) with $\mathrm{Ra} = 10^8$ and $\mathrm{Pr} = 1$: temporal evolution of (a) total kinetic energy $E_u(t)$, (b) total entropy $E_\theta(t)$.

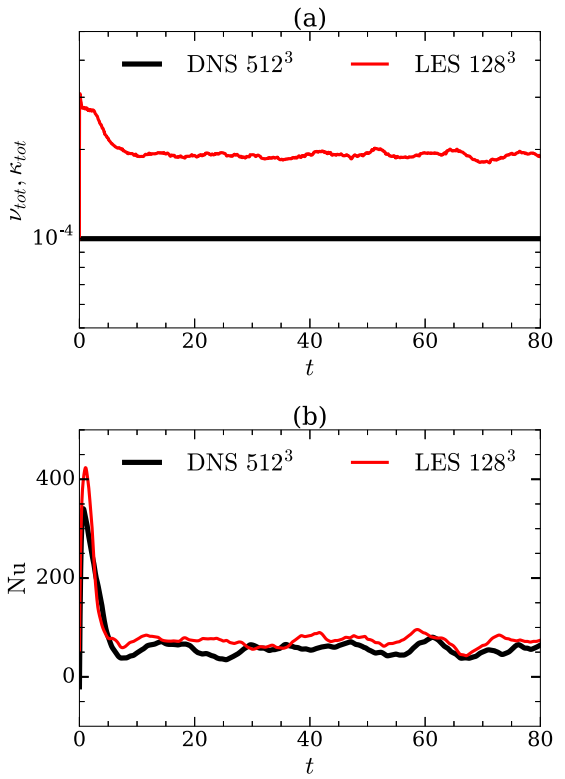


FIG. 2. Plots for LES on a $128^3$ grid (thin red lines) and DNS on a $512^3$ grid (thick black lines) with $\mathrm{Ra} = 10^8$ and $\mathrm{Pr} = 1$: temporal evolution of (a) total viscosity $\nu_{\mathrm{tot}}$, (b) Nusselt number Nu. Note that $\nu_{\mathrm{tot}} = \nu$ for DNS.

and (26). Thus, $\nu_{\mathrm{tot}}$ and $\kappa_{\mathrm{tot}}$ of LES are larger than that for DNS.

We start a DNS of RBC on a $512^3$ grid with a random initial condition. We consider a one-dimensional kinetic energy spectrum of Pope [55] and then choose random phases for the velocity Fourier modes. The Fourier modes of temperature field also have random phases. We start the LES on a $128^3$ grid by choosing the same Fourier modes as DNS for the resolved scales in LES [see Eqs. (27) and (28)]. This is the initial time, $t = 0$, of our simulation.

The equations are time advanced using fourth-order Runge-Kutta method. The Courant-Friedrichs-Lewy (CFL) condition is used to determine the time step $\Delta t$. The simulations are continued till 80 free-fall time units, $d/U$, where $d$ is the box height and $U = \sqrt{\alpha g \Delta d}$ is the free-fall time for the plumes. We observe that both DNS and LES reach a steady state at approximately 20 free-fall time units. In the following section we compare the results of the above DNS and LES.

## IV. COMPARISON OF DNS AND LES RESULTS

In this section, we compare the DNS and LES results on the evolution of global quantities such as total kinetic energy $(u^2/2)$, entropy $(\theta^2/2)$, and Nusselt number. We also compare the spectra and fluxes of kinetic energy and entropy, and the mean and rms profiles of temperature, as well as rms values of the vertical velocity, along the buoyancy direction, and the isosurfaces of temperature.

We start with the evolution of total energy $[E_u(t)]$ and entropy $[E_\theta(t)]$, which are defined as

$$E_{u,\mathrm{DNS}}(t) = \frac{1}{2}\sum_k |\hat{\mathbf{u}}(\mathbf{k})|^2; \tag{39}$$

$$E_{u,\mathrm{LES}}(t) = \frac{1}{2}\sum_k |\hat{\bar{\mathbf{u}}}(\mathbf{k})|^2, \tag{40}$$

$$E_{\theta,\mathrm{DNS}}(t) = \frac{1}{2}\sum_k |\hat{\theta}(\mathbf{k})|^2; \tag{41}$$

$$E_{\theta,\mathrm{LES}}(t) = \frac{1}{2}\sum_k |\hat{\bar{\theta}}(\mathbf{k})|^2. \tag{42}$$

In Figs. 1(a) and 1(b) we present $E_u(t)$ and $E_\theta(t)$ for DNS and LES. We observe that the steady states $E_u(t)$ and $E_\theta(t)$

TABLE I. Averaged quantities for our DNS and LES. Averaging was performed for $t = 30-80$.

| Case | Grid | Ra | $E_u$ | $E_\theta$ | Nu | $\nu_{\mathrm{tot}}$ |
|---|---|---|---|---|---|---|
| DNS | $128^3$ | $10^8$ | $(2.20 \pm 0.33)$e$-2$ | $(3.75 \pm 0.26)$e$-2$ | $55.5 \pm 10.7$ | $(1 \pm 0.047)$e$-4$ |
| LES | $512^3$ | $10^8$ | $(2.51 \pm 0.31)$e$-2$ | $(3.64 \pm 0.23)$e$-2$ | $72.4 \pm 10.9$ | 1.91e$-4$ |

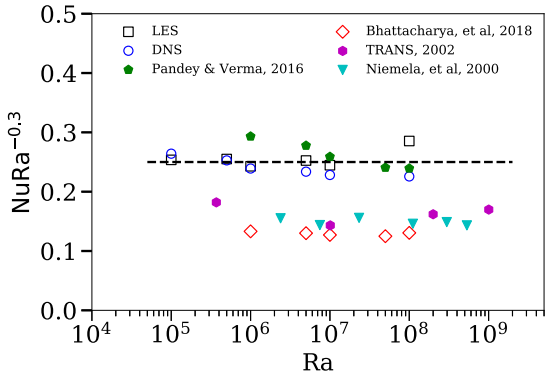


FIG. 3. Comparison of Nu-Ra scaling of our DNS and LES with the DNS by Pandey and Verma [49] for free-slip boundary condition, the DNS by Bhattacharya *et al.* [56] for no-slip boundary condition, the transient Reynolds-averaged Navier Stokes (TRANS) runs by Kenjereš and Hanjalic [27], and the experiments by Niemela *et al.* [57]. We plot $\mathrm{NuRa}^{-0.3}$ vs Ra. The dashed line denotes $\mathrm{NuRa}^{-0.3} = 0.25$. The exponents and coefficients of these runs are listed in Table II.

for LES and DNS are very similar. In Table I we list the average kinetic energy, entropy, Nusselt number, and $\nu_{\mathrm{tot}}$ with averaging performed over $t = 30$ to 80. Note that the total kinetic energy $E_u$ of LES, which is under-resolved, is marginally larger than that in DNS. This is because in the

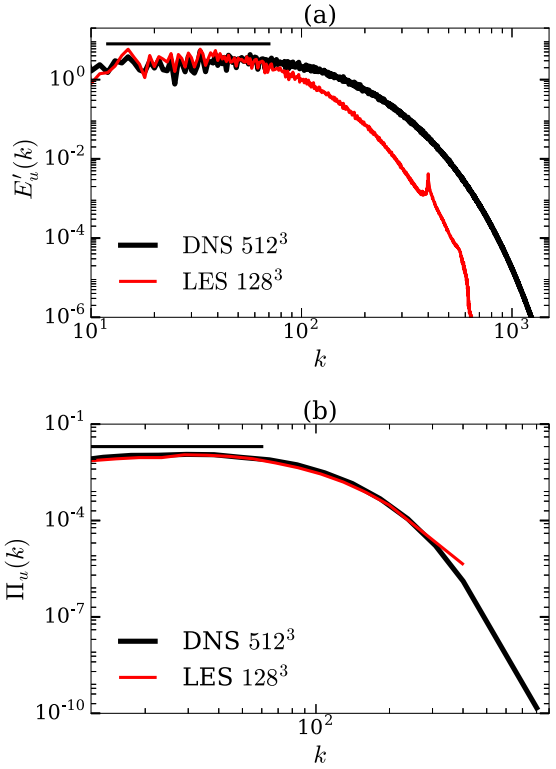


FIG. 4. Plots for LES (thin red lines) and DNS (thick black lines) of RBC with $\mathrm{Ra} = 10^8$ and $\mathrm{Pr} = 1$ at $t = 45$ free-fall time: (a) normalized kinetic energy spectrum $E'_u(k) = E_u(k)k^{5/3}\Pi^{-2/3}$, (b) kinetic energy flux $\Pi_u(k)$. We observe these quantities to be approximate constants (see flat line) in the inertial range $k = [10, 70]$.

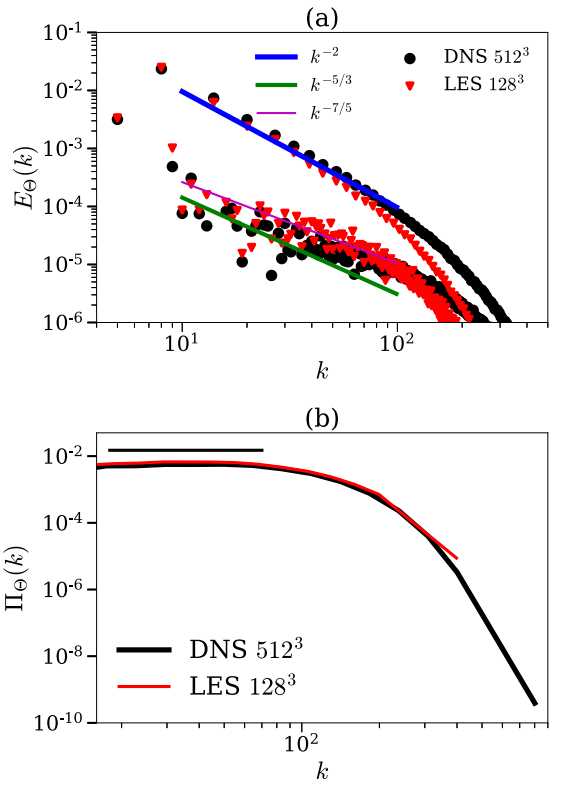


FIG. 5. Plots for LES and DNS of RBC with $\mathrm{Ra} = 10^8$ and $\mathrm{Pr} = 1$ at $t = 45$ free-fall time: (a) entropy spectra $E_\theta(k)$ exhibit a bispectrum where the upper branch scales as $k^{-2}$ (thick blue line), while the lower branch is fluctuating with neither $k^{-5/3}$ (green line with medium thickness) nor $k^{-3/2}$ spectrum (thin pink line). Red triangles represent LES, and black circles represent DNS. (b) Entropy flux $\Pi_\theta(k)$ is constant in the inertial range with the thick black line representing the DNS, and the thin red line representing the LES.

inertial range, $E_u(k)$ of LES is larger than that of DNS (to be discussed later in this section).

In Fig. 2(a) we compare the temporal evolution of total viscosity, $\nu_{\mathrm{tot}}$, of LES with $\nu = \sqrt{\mathrm{Pr}/\mathrm{Ra}}$ of DNS. As shown in Eq. (19) of the previous section, $\nu_{\mathrm{tot}}$ for LES is higher than that of DNS due to the additional renormalized viscosity, $\nu_{\mathrm{ren}}$.

The Nusselt number, Nu, is a ratio of total heat flux (convective and conductive) and conductive heat flux:

$$\mathrm{Nu} = \frac{\kappa(\Delta T)/d + \langle u_z\theta\rangle_V}{\kappa(\Delta T)/d}, \tag{43}$$

where $\langle\rangle_V$ represents volume average. The evolution of steady Nu for LES shown in Fig. 2(b) closely follows the results from DNS, especially after attaining steady-state flow. From Table I we infer that for $\mathrm{Ra} = 10^8$, the average Nu of LES exceeds that of DNS by approximately 30%; this increase as well as larger Nu exponent are similar to earlier LES results [30,32,34,37], and they can be attributed to the absence of backscatter in LES.

In Fig. 3 we compare our LES and DNS results for Nu with those from DNS with free-slip boundary condition [49], DNS with no-slip boundary condition [56], TRANS simulation [27], and an experiment [57]. Table II contains Nu scaling

TABLE II. Comparison of Nu-Ra scaling for different simulations: $a$, $b$ of $\mathrm{Nu} = a\mathrm{Ra}^b$, range of Rayleigh number (Ra) and Prandtl numbers (Pr), aspect ratio (A.R.), and boundary condition (B.C.). The different boundary conditions listed are free-slip velocity B.C.'s in the vertical direction and periodic B.C.'s along horizontal directions (B1), stress-free velocity B.C.'s in all directions (B2), no-slip B.C.'s in all directions (B3), and no-slip B.C.'s in vertical direction and periodic BCs along the horizontal directions (B4).

| Case | $a$ | $b$ | Ra | Pr | A.R. | B.C. |
|---|---|---|---|---|---|---|
| Present DNS | 0.29 | 0.28 | $10^5$–$10^8$ | 0.5–5.0 | 1 | B1 |
| Present LES | 0.14 | 0.33 | $10^5$–$10^8$ | 0.5–5.0 | 1 | B1 |
| Pandey and Verma [49] (DNS) | 0.54 | 0.25 | $10^6$–$10^8$ | 1 | 1 | B3 |
| Bhattacharya *et al.* [56] (DNS) | 0.12 | 0.30 | $10^6$–$10^8$ | 1 | 1 | B3 |
| Sergent *et al.* [33] (LES) | 0.13 | 0.30 | $6.3 \times 10^5$–$2 \times 10^{10}$ | 0.71 | 6 and 4 | B4 |
| Kimmel and Domaradzki [37] (LES) | 0.21 | 0.28 | $6.3 \times 10^5$–$10^8$ | 1 | 6 | B4 |
| Eidson [30] (LES) | - | 0.28 | $10^5$–$2.5 \times 10^6$ | 0.71 | 4 | B4 |
| Vincent and Yuen [21] (2D-DNS) | - | $\approx 1/3$ | $10^8$–$10^{10}$ | 1 | 3 | B2 |

results of some of the earlier DNS and LES studies. We observe that $\mathrm{Nu} = 0.29\mathrm{Ra}^{0.28}$ for our DNS and $\mathrm{Nu} = 0.14\mathrm{Ra}^{0.33}$ for our LES, and they are approximately in the same range as the earlier results.

Kooij *et al.* [19] reported that $\mathrm{Nu} \approx 32$ for turbulent convection in a cylinder with $\mathrm{Pr} = 1$ and $\mathrm{Ra} = 10^8$ under no-slip boundary condition. Our Nu is larger than that of Kooij *et al.* [19], and this is due to the different boundary conditions employed in our simulations. The Nu-Ra exponent of our LES is larger than those of Kimmel and Domaradzki [37] and Eidson [30] for the same reason. It has been argued earlier that RBC with no-slip boundary condition has a smaller Nu than its free-slip counterpart because the flow in no-slip RBC face more resistance due to viscous boundary layers [58]. We observe a deviation in the average Nu, especially at high Ra, and this could possibly be due to the random emergence of large-scale plumes with long timescales (see the time series of Figs. 1 and 2).

Figures 4(a) and 4(b) exhibits the normalized kinetic energy spectra $E'_u(k) = E_u(k)k^{5/3}\Pi_u^{2/3}$ and the kinetic energy fluxes $\Pi_u(k)$ at $t = 45$ for DNS and LES. In the inertial range, $E'_u(k)$ is approximately constant for DNS and LES, and their values are close to each other; these results are consistent with those of Kumar *et al.* [46] and Verma *et al.* [18], who showed that turbulent thermal convection exhibits Kolmogorov's 5/3 scaling. The kinetic energy flux $\Pi_u(k)$ is also constant in the

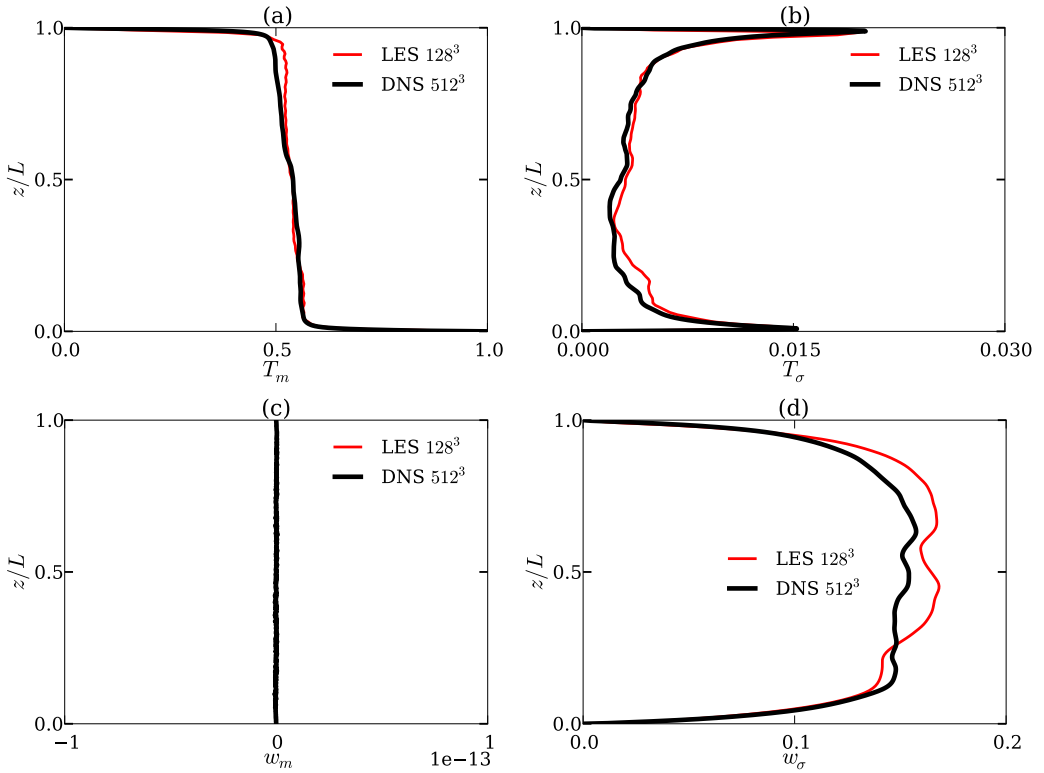


FIG. 6. Plots for LES (thin red lines) and DNS (thick black lines) of RBC with $\mathrm{Ra} = 10^8$ and $\mathrm{Pr} = 1$: (a) horizontally averaged temperature $T_m(z)$; (b) planar averaged rms values of the temperature, $T_\sigma(z)$; (c) planar averaged vertical velocity, $w_m(z)$, which is 0 due to continuity and wall constraint; (d) planar averaged rms values of the vertical velocity, $w_\sigma(z)$.

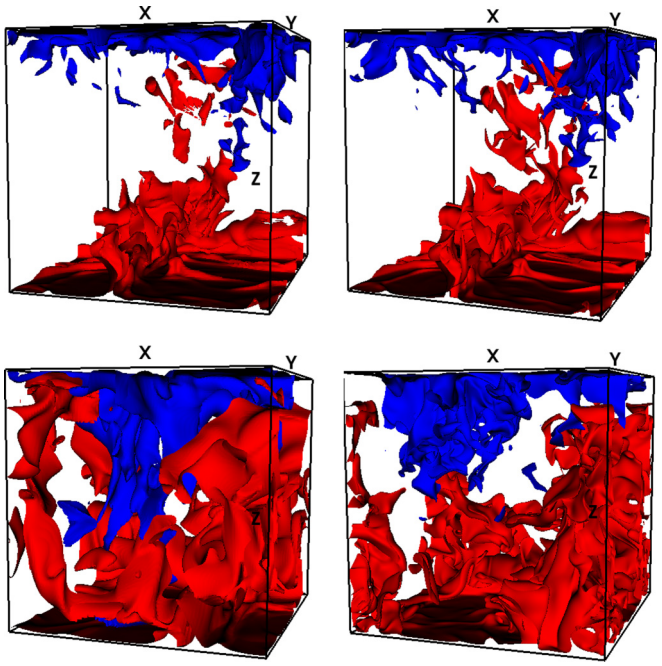


FIG. 7. Plots for LES and DNS of RBC with Ra $= 10^8$ and Pr $=$ 1: The temperature isosurfaces at $t = 45$ (top row) and at $t = 80$ (bottom row). The left configurations represent the LES profiles, while those on the right are from DNS.

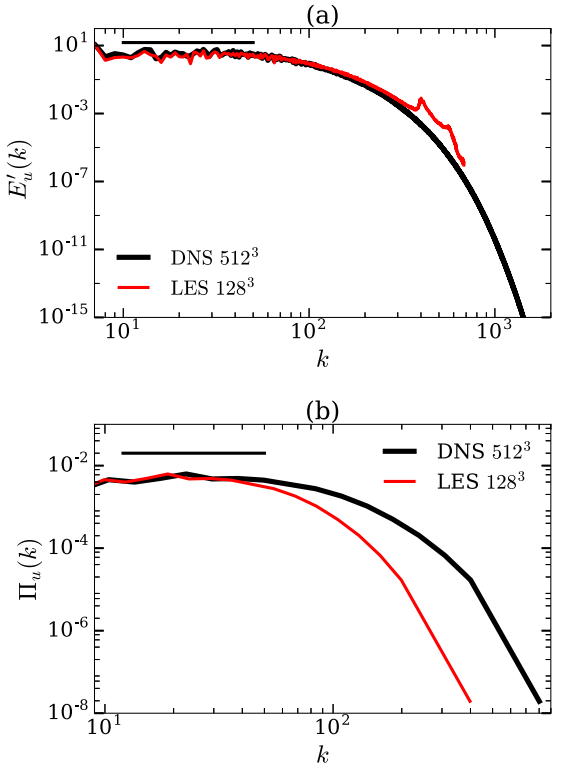


FIG. 8. Plots for LES (thin red lines) and DNS (thick black lines) of RBC with Ra $= 10^7$ and Pr $= 0.5$ at $t = 45$ free-fall time: (a) normalized kinetic energy spectrum; (b) kinetic energy flux $\Pi_u(k)$.

inertial range ($k = [10, 70]$), consistent with the above results of $E'_u(k)$. The dissipation range $E'_u(k)$ of LES is, however, lower than its DNS counterpart due to lower resolution of LES. The energy flux, however, for LES and DNS is approximately the same till $k = k_c = (2\pi/3)128 \approx 270$, where the cutoff for LES is employed. Also note that, in the inertial range, $E'_u(k)$ for LES is marginally higher than that in DNS. This leads to increase in total $E_u$ for LES compared to that in DNS.

In Fig. 5 we plot the entropy spectra and fluxes computed using the LES and DNS data at $t = 45$. Note that the LES, similar to DNS, captures the bispectrum of $E_\theta(k)$. Here the upper branch exhibits $k^{-2}$ spectrum, whereas the lower branch is fluctuating. Mishra and Verma [59] and Pandey *et al.* [58] had shown that the upper $k^{-2}$ branch is constituted by the dominant temperature modes $\theta(0, 0, 2n)$, which are approximately $-1/2\pi n$. Furthermore, the temperature modes in these two branches interact in such a way as to yield a constant entropy flux in the inertial regime. As shown in Fig. 5(b), $\Pi_\theta(k)$ obtained through LES exhibits a similar behavior as DNS. Thus, the role of dominant temperature modes and the interactions among these modes is properly captured by our LES.

So far, we have compared LES and DNS results for the global and spectral quantities. We find that our LES also captures the real space profile of DNS well. In Figs. 6(a) and 6(b) we plot the horizontally averaged temperature, $T_m(z)$, and planar rms values of the temperature, $T_\sigma(z)$. Figure 6(c) contains the rms value of the vertical velocity. In addition, for better smoothing, we time average the above quantities over four eddy-turnover times. We observe a good agreement between the DNS and LES results of the above quantities.

Finally, Fig. 7 exhibits the isosurfaces of temperature obtained in DNS and LES at $t = 45$ (top row) and at $t = 80$ (bottom row) free-fall time units. The LES results are in the left column, and the DNS results are in the right column. Note the similarity between the resolved structures in the two figures. Thus, the spatial structures of resolved scales are captured by the LES.

It is important to note that for Ra $= 10^8$, DNS at the resolution of $128^3$ could not be performed since the $128^3$ grid is too small to resolve flow structures for such large Ra. A DNS on this grid diverges very quickly, and hence, we could not compare DNS and LES on a $128^3$ grid.

In the present section we discussed comparative results of LES and DNS for molecular Prandtl number of unity and Ra $= 10^8$. As we argued in Sec. II, our LES scheme is expected to work for moderate Prandtl numbers. To test this conjecture, we performed comparative tests for molecular Prandtl numbers Pr $= 5$ and 0.5 (both with Ra $= 10^8$). We observe that the inertial range behavior of DNS and LES is similar. These results are described in Appendix A.

## V. CONCLUSIONS

In this paper, we present a SGS model for LES of turbulent thermal convection that employs renormalized viscosity and thermal diffusivity. The LES scheme makes use of the fact that the behavior of turbulent thermal convection is similar to that of hydrodynamic turbulence [18,46]. Using this scheme we performed LES on a $128^3$ grid at a Rayleigh

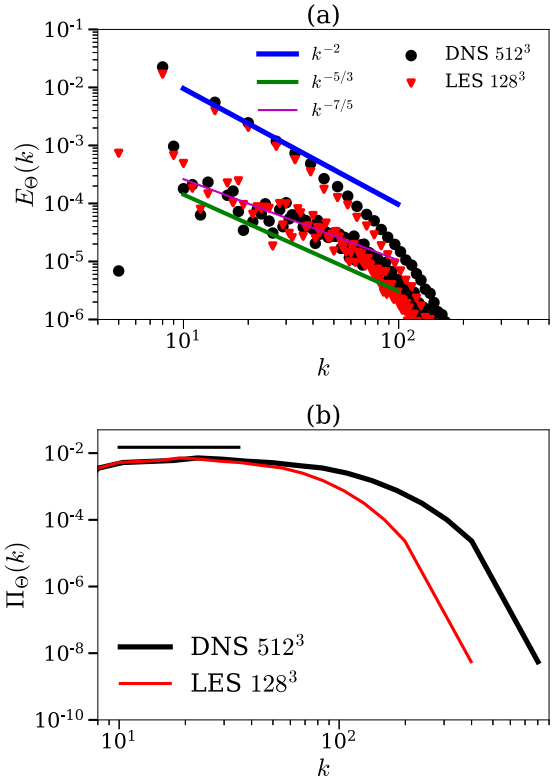


FIG. 9. Plots for LES and DNS of RBC with $\mathrm{Ra} = 10^7$ and $\mathrm{Pr} = 0.5$ at $t = 45$ free-fall time: (a) entropy spectrum $E_\theta(k)$ exhibiting bispectra with red triangles for LES and black circles for DNS. The blue, green, and pink lines with decreasing thickness represent $k^{-2}$, $k^{-5/3}$, and $k^{-7/5}$ curves; (b) entropy flux $\Pi_\theta(k)$ with the thick black line representing the DNS, and the thin red line representing the LES.

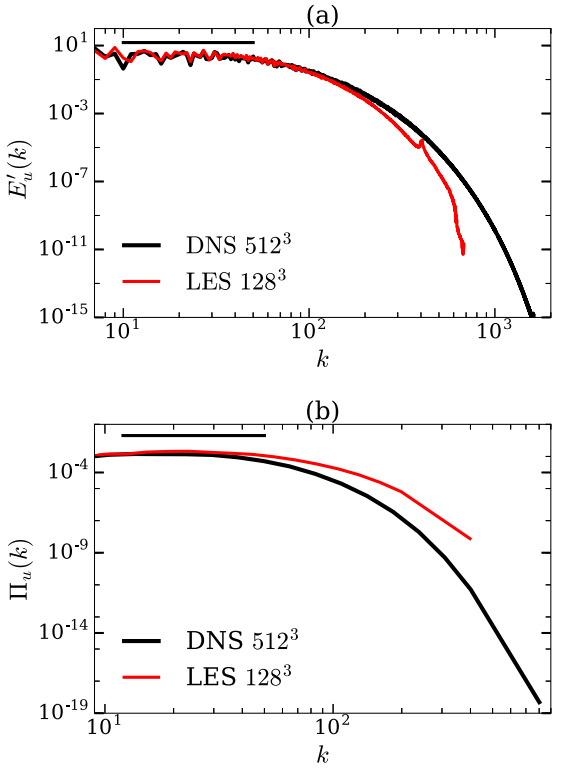


FIG. 10. Plots for LES (thin red lines) and DNS (thick black lines) of RBC with $\mathrm{Ra} = 10^8$ and $\mathrm{Pr} = 5.0$ at $t = 45$ free-fall time: (a) normalized kinetic energy spectrum $E'_u(k) = E_u(k)k^{5/3}\Pi^{-2/3}$; (b) kinetic energy flux $\Pi_u(k)$.

number of $10^8$ and a molecular Prandtl number of unity. We compared the LES results with those of DNS on a $512^3$ grid for the same parameters. We observe that, in the inertial range, the spectra and fluxes of kinetic energy and entropy are approximately the same. The global quantities—total kinetic energy, entropy, and Nusselt number—also evolve in a similar manner as in the DNS. However, the Nusselt number for LES is larger than that of DNS (see Table I), and this observation is consistent with earlier works [30,32,34,37]. Besides this, the LES could capture the large-scale structures of DNS very well.

The present LES scheme uses the same dissipative coefficients for the whole fluid, which can be improved considering different flow behavior in the bulk and in the boundary layer. Inclusion of variable dissipative coefficients requires more sophisticated modeling of the viscosity and thermal diffusivity in the bulk and in the boundary layer. Note that the local energy flux is expected to be different at different locations, especially in the bulk and in the boundary layer. Hence, we need to model the energy flux $\Pi_u$ of Eq. (19) locally. This could possibly be computed using the third-order structure function [60]. Also, we need to test our scheme for RBC with much larger Ra's. Simulation of the ultimate regime [61] would require further tweaks. We plan to attempt such generalizations and investigations in the near future.

The present LES model is expected to work well for moderate molecular Prandtl numbers, e.g., between 0.1 and 10, because both velocity and temperature fields are turbulent in this regime. We demonstrate this by showing good agreement between the LES and DNS results for $\mathrm{Pr} = 0.5$ and 5. Note that the flow behavior is quite different for very large and very small Prandtl numbers. The equation for the velocity field becomes linear for very large Pr, [58], while that for the temperature field becomes linear for very small Pr [59]. As a result, the LES scheme needs to be appropriately modified for RBC simulations with extreme Prandtl numbers.

In summary, the present LES scheme for turbulent thermal convection captures the results of DNS—global kinetic energy, inertial-range kinetic energy and flux, etc. We hope to be able to extend our LES to model the bulk and the boundary layers of the flow, as well as simulate RBC with the extreme Prandtl numbers.

## ACKNOWLEDGMENTS

We thank Fahad Anwer, Abhishek Kumar, Anando Chatterjee, Shashwat Bhattacharya, Manohar Sharma, and Mohammad Anas for useful discussions. We are grateful to the anonymous referees for their insightful comments. The simulations were performed on the HPC system and Chaos cluster of IIT Kanpur, India, and the Shaheen supercomputer at King Abdullah University of Science and Technology (KAUST), Saudi Arabia. This work was supported by research grants PLANEX/PHY/2015239 from the Indian Space

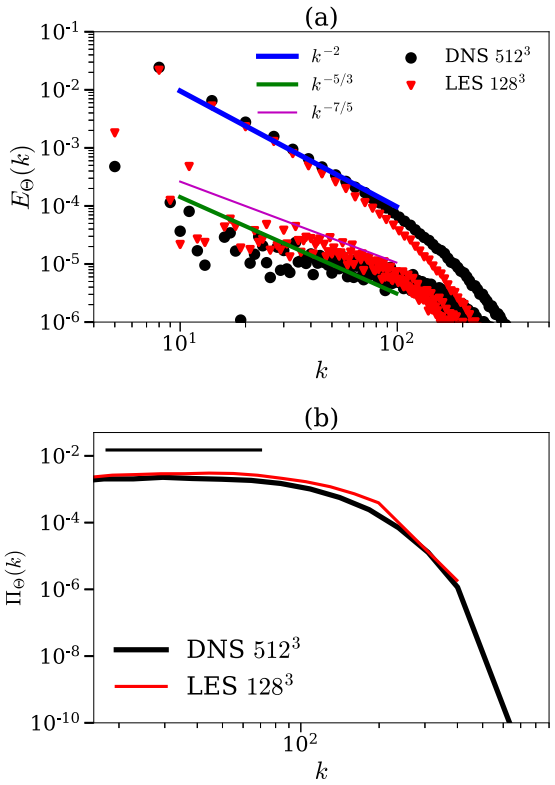


FIG. 11. Plots for LES and DNS of RBC with $\mathrm{Ra} = 10^8$ and $\mathrm{Pr} = 5.0$ at $t = 45$ free-fall time: (a) entropy spectrum $E_\theta(k)$ exhibiting bispectra with red triangles for LES and black circles for DNS. The blue, green, and pink lines with decreasing thickness represent $k^{-2}$, $k^{-5/3}$, and $k^{-7/5}$ curves; (b) entropy flux $\Pi_\theta(k)$ with the thick black line representing the DNS, and the thin red line representing the LES.

Research Organisation (ISRO), India, and project K1052 by KAUST.

## APPENDIX

In the main text we described LES results for a molecular Prandtl number of unity. The proposed scheme, however, is general, and it is expected to work for moderate Prandtl numbers between 0.1 and 10 (see Sec. II). To test this conjecture, we performed DNS and LES for two additional Prandtl numbers: 0.5 at $\mathrm{Ra} = 10^7$ and 5.0 at $\mathrm{Ra} = 10^8$; the results from these simulations are presented in this Appendix.

Following the discussion of Sec. II, we take $\kappa_{\mathrm{ren}} = \nu_{\mathrm{ren}}$. Following Eq. (24), we obtain

$$\mathrm{Pr}_{\mathrm{tot}} = \frac{\nu + \nu_{\mathrm{ren}}}{\kappa + \kappa_{\mathrm{ren}}} = \frac{\nu + \nu_{\mathrm{ren}}}{\kappa + \nu_{\mathrm{ren}}}. \tag{A1}$$

Since $\nu \ll \nu_{\mathrm{ren}}$, and $\kappa \ll \kappa_{\mathrm{ren}}$, we expect that $\mathrm{Pr}_{\mathrm{tot}}$ is marginally greater than unity for molecular Prandtl number of 5, and marginally smaller than unity for that of $\mathrm{Pr} = 0.5$. We perform our DNS and LES following the same scheme as described in Sec. III.

In Figs. 8 and 9 we present the spectra and fluxes for $\mathrm{Pr} = 0.5$. Figures 10 and 11 exhibit the corresponding plots for $\mathrm{Pr} = 5.0$. In the inertial range, the LES results are in good agreement with those for DNS. This is satisfactory because LES is designed to resolve the large-scale and inertial range physics. Note however minor discrepancies in the spectra and flux plots in dissipative range. LES is not expected to resolve the dissipative range, yet we may be able to model this using appropriate choice of diffusion parameters. In the future, we plan to tweak our renormalized viscosity and diffusivity as $\kappa_{\mathrm{ren}} = C\nu_{\mathrm{ren}}$ with $C$ as a free parameter.

We have also computed the Nusselt numbers for $\mathrm{Pr} = 0.5$ and 5. For $\mathrm{Pr} = 0.5$, Nu for LES and DNS are 27.2 and 26.4, respectively. The corresponding numbers for $\mathrm{Pr} = 5$ are 111 and 75.4, respectively.


[1] J. Smagorinsky, Month. Weather Rev. **91**, 99 (1963).
[2] V. Yakhot and S. A. Orszag, J. Sci. Comput. **1**, 3 (1986).
[3] W. D. McComb and A. G. Watt, Phys. Rev. A **46**, 4797 (1992).
[4] W. D. McComb, *The Physics of Fluid Turbulence* (Clarendon Press, Oxford, 1990).
[5] W. D. McComb, *Homogeneous, Isotropic Turbulence: Phenomenology, Renormalization and Statistical Closures* (Oxford University Press, Oxford, 2014).
[6] Y. Zhou, G. Vahala, and M. Hossain, Phys. Rev. A **37**, 2590 (1988).
[7] Y. Zhou, Phys. Rep. **488**, 1 (2010).
[8] M. K. Verma, Phys. Rep. **401**, 229 (2004).
[9] M. K. Verma and S. Kumar, Pramana-J. Phys. **63**, 553 (2004).
[10] S. Vashishtha, A. Chatterjee, A. Kumar, and M. K. Verma, arXiv:1712.03170 [physics.flu-dyn] (2017).
[11] G. Ahlers, S. Grossmann, and D. Lohse, Rev. Mod. Phys. **81**, 503 (2009).
[12] D. Lohse and K.-Q. Xia, Annu. Rev. Fluid Mech. **42**, 335 (2010).
[13] M. K. Verma, *Physics of Buoyant Flows: From Instabilities to Turbulence* (World Scientific, Singapore, 2018).
[14] R. J. A. M. Stevens, Q. Zhou, S. Grossmann, R. Verzicco, K.-Q. Xia, and D. Lohse, Phys. Rev. E **85**, 027301 (2012).
[15] O. Shishkina, S. Horn, S. Wagner, and E. S. C. Ching, Phys. Rev. Lett. **114**, 114302 (2015).
[16] O. Shishkina and A. Thess, J. Fluid Mech. **633**, 449 (2009).
[17] O. Shishkina, R. J. Stevens, S. Grossmann, and D. Lohse, New J. Phys. **12**, 075022 (2010).
[18] M. K. Verma, A. Kumar, and A. Pandey, New J. Phys. **19**, 025012 (2017).
[19] G. L. Kooij, M. A. Botchev, E. M. Frederix, B. J. Geurts, S. Horn, D. Lohse, E. P. van der Poel, O. Shishkina, R. J. Stevens, and R. Verzicco, Comput. Fluids **166**, 1 (2018).
[20] X. Zhu, V. Mathai, R. J. A. M. Stevens, R. Verzicco, and D. Lohse, Phys. Rev. Lett. **120**, 144502 (2018).
[21] A. P. Vincent and D. A. Yuen, Phys. Rev. E **61**, 5241 (2000).
[22] J. Schumacher, V. Bandaru, A. Pandey, and J. D. Scheel, Phys. Rev. Fluids **1**, 084402 (2016).

[23] K. L. Chong, S. Wagner, M. Kaczorowski, O. Shishkina, and K.-Q. Xia, Phys. Rev. Fluids **3**, 013501 (2018).
[24] G. Grötzbach, J. Fluid Mech. **119**, 27 (1982).
[25] G. Grötzbach, J. Comput. Phys. **49**, 241 (1983).
[26] K. Hanjalić, Annu. Rev. Fluid Mech. **34**, 321 (2002).
[27] S. Kenjereš and K. Hanjalic, Phys. Rev. E **66**, 036307 (2002).
[28] X. Chavanne, F. Chillà, B. Chabaud, B. Castaing, and B. Hebral, Phys. Fluids **13**, 1300 (2001).
[29] X. He, D. Funfschilling, H. Nobach, E. Bodenschatz, and G. Ahlers, Phys. Rev. Lett. **108**, 024502 (2012).
[30] T. M. Eidson, J. Fluid Mech. **158**, 245 (1985).
[31] X.-J. Huang, L. Zhang, Y.-P. Hu, and Y.-R. Li, Fluid Dyn. Res. **50**, 035503 (2018).
[32] F. Dabbagh, F. Trias, A. Gorobets, and A. Oliva, Phys. Fluids **29**, 105103 (2017).
[33] A. Sergent, P. Joubert, and P. L. Quere, Prog. Comp. Fluid Dyn. **6**, 40 (2006).
[34] V. C. Wong and D. K. Lilly, Phys. Fluids **6**, 1016 (1994).
[35] N. Foroozani, J. J. Niemela, V. Armenio, and K. R. Sreenivasan, Phys. Rev. E **95**, 033107 (2017).
[36] C. Meneveau, T. S. Lund, and W. H. Cabot, J. Fluid Mech. **319**, 353 (1996).
[37] S. J. Kimmel and J. A. Domaradzki, Phys. Fluids **12**, 169 (2000).
[38] O. Shishkina and C. Wagner, Phys. Fluids **19**, 085107 (2007).
[39] O. Shishkina and C. Wagner, J. Fluid Mech. **599**, 383 (2008).
[40] A. Leonard and G. Winckelmans, A tensor-diffusivity subgrid model for large-eddy simulation, Technical report cit-asci-tr043 (1999).
[41] U. Piomelli, W. H. Cabot, P. Moin, and S. Lee, Phys. Fluids A **3**, 1766 (1991).
[42] D. Nath, A. Pandey, A. Kumar, and M. K. Verma, Phys. Rev. Fluids **1**, 064302 (2016).
[43] V. S. L'vov, Phys. Rev. Lett. **67**, 687 (1991).
[44] V. S. L'vov and G. Falkovich, Physica D **57**, 85 (1992).
[45] R. Rubinstein, Renormalization group theory of Bolgiano scaling in Boussinesq turbulence, Technical report ICOM-94-8; CMOTT-94-2 (1994).
[46] A. Kumar, A. G. Chatterjee, and M. K. Verma, Phys. Rev. E **90**, 023016 (2014).
[47] S. Chandrasekhar, *Hydrodynamic and Hydromagnetic Stability* (Oxford University Press, Oxford, 2013).
[48] M. K. Verma, Int. J. Mod. Phys. B **15**, 3419 (2001).
[49] A. Pandey and M. K. Verma, Phys. Fluids **28**, 095105 (2016).
[50] V. Borue and S. A. Orszag, J. Sci. Comput. **12**, 305 (1997).
[51] G. Dar, M. K. Verma, and V. Eswaran, Physica D **157**, 207 (2001).
[52] M. K. Verma, A. G. Chatterjee, R. K. Yadav, S. Paul, M. Chandra, and R. Samtaney, Pramana-J. Phys. **81**, 617 (2013).
[53] A. G. Chatterjee, M. K. Verma, A. Kumar, R. Samtaney, B. Hadri, and R. Khurram, J. Parallel Distrib. Comput. **113**, 77 (2018).
[54] C. Canuto, M. Y. Hussaini, A. Quarteroni, and T. A. Zang, *Spectral Methods in Fluid Dynamics* (Springer-Verlag, Berlin, 1988).
[55] S. B. Pope, *Turbulent Flows* (Cambridge University Press, Cambridge, 2000).
[56] S. Bhattacharya, A. Pandey, A. Kumar, and M. K. Verma, Phys. Fluids **30**, 031702 (2018).
[57] J. J. Niemela, L. Skrbek, K. R. Sreenivasan, and R. J. Donnelly, Nature (London) **404**, 837 (2000).
[58] A. Pandey, M. K. Verma, and P. K. Mishra, Phys. Rev. E **89**, 023006 (2014).
[59] P. K. Mishra and M. K. Verma, Phys. Rev. E **81**, 056316 (2010).
[60] U. Frisch, *Turbulence: The Legacy of A. N. Kolmogorov* (Cambridge University Press, Cambridge, 1995).
[61] R. H. Kraichnan, Phys. Fluids **5**, 1374 (1962).